

$\rho \rightarrow \pi\pi$ decay in nuclear medium[★]

Wojciech Broniowski^a, Wojciech Florkowski^a, Brigitte Hiller^b

^a *The H. Niewodniczański Institute of Nuclear Physics, PL-31342 Cracow, Poland*

^b *Centro de Física Teórica, University of Coimbra, P-3004 516 Coimbra, Portugal*

We calculate the medium modifications of the $\rho\pi\pi$ vertex in a relativistic hadronic framework incorporating nucleons and $\Delta(1232)$ isobars, and find a substantial increase of the $\rho\pi\pi$ coupling, dominated by processes where the Δ is excited. The coupling depends significantly on the virtuality of the ρ , which is related to analytic properties of the vertex function. We analyze the general case of a non-zero three-momentum of the ρ with respect to the nuclear medium, and evaluate the resulting widths and spectral strength in the transverse and longitudinal channels for the $\rho \rightarrow \pi\pi$ decay. These widths are used to obtain the dilepton yields from ρ decays in relativistic heavy-ion collisions.

Keywords: Mesons in nuclear medium, dilepton production in relativistic heavy-ion collisions

PACS: 25.75.Dw, 21.65.+f, 14.40.-n

1 Introduction

In recent years a lot of efforts have been undertaken in order to understand the properties of hadrons in nuclear medium. This challenging theoretical issue gains a lot of importance at the beginning of the operation of RHIC, where a proper and accurate inclusion of hadrons is necessary to describe the evolution of the “hadronic soup” formed in the collision. It is commonly accepted that hadrons are significantly modified by nuclear matter. The arguments range

[★] Research supported by PRAXIS grants XXI/BCC/429/94, PRAXIS/P/FIS/12247-/1998, by Fundação para a Ciência e a Tecnologia, POCTI/2000/FIS/35304, and by the Polish State Committee for Scientific Research grant 2P03B09419.

^{★★} E-mail: Wojciech.Broniowski@ifj.edu.pl, brigitte@teor.fis.uc.pt, Wojciech.Florkowski@ifj.edu.pl

from simple scaling of masses [1,2], through numerous hadronic model calculations [3,4,5,6,7,8,9,10,11,12,13,14,15,16,17], QCD sum-rule techniques [18,19,20], approaches motivated by the chiral symmetry [21,22,23,24,25,26,27,28], to model-independent predictions based on low-density expansion and dispersion relations [29,30,31,32]. In these calculations masses of hadrons, or widths, or both, are significantly changed by the presence of the medium (for a recent review see [33,34,35]). In addition, medium may induce meson mixing absent in the vacuum [36,37,38,39]. An indirect indication for the modification of vector mesons has been provided by the dilepton production measurements in relativistic heavy-ion collisions (CERES [40], HELIOS [41]). The dilepton productions has been theoretically studied with medium-modified vector mesons [42,43,44,45,46,47], which helps to explain the low-mass enhancement of the dilepton yields.

There is a lot of studies of the meson two-point functions in the literature, but only a few devoted to meson three-point functions. In their study of the ρ -meson in-medium spectral function Herrmann, Friman, and Nörenberg [7] have computed the $\rho\pi\pi$ vertex for the ρ at rest in nuclear matter. They have applied a hadronic model with the Δ isobar and with non-relativistic couplings. Temperature effects on the $\rho\pi\pi$ interaction have been considered by Song and Koch [48]. Urban, Buballa, Rapp and Wambach [11,12] have extended the calculation of Ref. [7] to non-zero three-momenta of the ρ meson and non-zero temperature. The authors of the present paper have analyzed the $\omega \rightarrow \pi\pi$ decay in nuclear medium [49,50,51]. Krippa has theoretically studied the effects of density on chiral mixing of meson three-point functions [52]. In Ref. [53] the $\rho\pi\pi$ coupling has been studied in quark matter. Otherwise, the topic of medium effects on hadronic couplings is very much *terra incognita*. Certainly, if the two-point functions are significantly altered by the medium, one expects that the three-point functions should also change. The issue is important for modeling the hadronic evolution in relativistic heavy-ion collisions, since the change of the hadron couplings results in altered transition rates between hadrons.

Out of many meson couplings, the $\rho\pi\pi$ vertex is especially important, since the ρ plays an essential role in hadron dynamics. The vacuum value of the coupling constant is large, $g_{\rho\pi\pi} \simeq 6$. Since the couplings of ρ and pions to nucleons and Δ isobars are also large, we expect significant medium modifications of $g_{\rho\pi\pi}$. As our calculation shows, this is indeed the case, with the coupling significantly altered already at the nuclear saturation density. The effect is mainly due to the interactions with the Δ . Our method is similar to Refs. [7,11], with the following differences: We use a *fully relativistic* framework, with relativistic interactions. The *leading-density* approximation is used, which makes the calculation very simple, as no integration over the nucleon momenta is necessary. We analyze analyticity in the virtual ρ mass, which is non-trivial in our problem due to low-mass thresholds. These thresholds largely influence the results. In addition,

keeping non-zero three-momentum of the ρ , as in Ref. [11], allows us to look separately on the longitudinal and transverse polarizations. In our comparison to the CERES dilepton data we use the fire-cylinder expansion model of Refs. [54,55] and take into account the experimental cuts, which are very important for the detailed numerical analysis.

The outline and the main results of the paper are as follows: In Sect. 2 we introduce our framework, *i.e.* the relativistic model of mesons interacting with nucleons and Δ isobars, the latter treated as Rarita-Schwinger fields. We introduce the necessary hadronic vertices and set the coupling constants. As already mentioned, we work at zero temperature and to the leading-order in baryon density. In Sect. 3 we present our results for the $\rho\pi\pi$ vertex for the ρ meson at rest with respect to the medium, and point out large medium effects even at the nuclear saturation density. We investigate analyticity of the coupling in the virtual ρ meson mass and point out its significance for the quantitative results. We look at effects of the energy-dependent width of the Δ and find they are not very large. In Sect. 4 we analyze the general case of finite three-momentum of the ρ with respect to the medium, and calculate the widths and spectral functions in the transverse and longitudinal channels. In Sect. 5 we apply the obtained spectral functions to compute the dilepton production rate from ρ decays for the CERES $Pb + Au$ experiment. The calculation carefully includes the CERES experimental kinematic cuts, which is crucial for the results. We also include the effects of the expansion of the fire cylinder, which enter at the level of a few percent. It is found that spreading of the width helps to explain the low-mass enhancement of the dilepton spectra, but the overall normalization fails significantly short of the experimental data. Section 6 presents our conclusions and a discussion of several additional points.

2 The framework

Throughout this paper we choose conventionally q as the incoming momentum of the ρ carrying isospin index b and polarization vector ε^μ , p as the outgoing momentum of the pion carrying isospin index a , and $q - p$ as the outgoing momentum of the pion carrying isospin index c . With this convention, the vacuum value of the $\rho\pi\pi$ vertex (Feynman rule) is

$$-iV_{\rho_\mu^b \pi^a \pi^c} = g_\rho \varepsilon^{acb} (2p^\mu - q^\mu). \quad (1)$$

The medium modifications of the coupling, calculated below, will be compared to Eq. (1).

Our calculation of the in-medium $\rho\pi\pi$ vertex is made in the framework of a fully relativistic hadronic theory, where mesons interact with the nucleons and Δ isobars. Other in-medium calculations indicate that the leading-density approximation is sufficient up to densities of the order of the nuclear saturation density.¹ Also, in Ref. [12] the finite-temperature effects in the $\rho\pi\pi$ coupling have been found to be moderate for temperatures up to about $\sim 150\text{MeV}$, typical for relativistic heavy-ion collisions (cf. Fig. 7(a,b) of [12]). This justifies the use of zero temperature to obtain the vertices of Fig. 1, at least as a first approximation.

To the leading-density order only the diagrams shown in Fig. 1 contribute to the $\rho \rightarrow \pi\pi$ process. The solid lines denote i times the in-medium nucleon propagator, which can be decomposed in the usual way into the *free* and *density* parts [4]:

$$\begin{aligned} iG(k) &\equiv iG_F(k) + iG_D(k) = \\ &= i(\not{k} + m_N) \left[\frac{1}{k^2 - m_N^2 + i\varepsilon} + \frac{i\pi}{E_k} \delta(k_0 - E_k) \theta(k_F - |\mathbf{k}|) \right], \end{aligned} \quad (2)$$

where k denotes the nucleon four-momentum, m_N is the nucleon mass, $E_k = \sqrt{m_N^2 + \mathbf{k}^2}$, and k_F is the Fermi momentum of nuclear matter. The double line in the diagrams of Fig. 1 denotes i times the relativistic Δ propagator,

$$iG_{\Delta}^{\alpha\beta}(k) = i \frac{\not{k} + m_{\Delta}}{k^2 - \left(m_{\Delta} - \frac{i}{2}\Gamma_{\Delta}\right)^2} \left(-g^{\alpha\beta} + \frac{1}{3}\gamma^{\alpha}\gamma^{\beta} + \frac{2k^{\alpha}k^{\beta}}{3m_{\Delta}^2} + \frac{\gamma^{\alpha}k^{\beta} - \gamma^{\beta}k^{\alpha}}{3m_{\Delta}} \right). \quad (3)$$

This formula corresponds to the usual Rarita-Schwinger definition [56,57], with the parameter choice $A = -1$. We have modified the denominator in Eq. (3) in order to account for the finite width of the Δ resonance.

Since we are interested in density effects, one of the nucleon lines in each of the diagrams of Fig. 1 must involve the nucleon density propagator, G_D . For kinematic reasons, diagrams with more than one G_D vanish. The wavy line in Fig. 1 denotes the ρ meson, and the dashed lines correspond to pions. All external particles are on mass shell.

The meson-nucleon vertices (Feynman rules) needed for our calculation have the standard form

¹ An extension beyond the leading-density approximation would require accounting for the Fermi-sea motion, which technically leads to keeping the integration over \mathbf{k} in our expressions, and, more importantly, the inclusion of correlations. In many similar calculations the Fermi-motion effects have been found to influence the results weakly at moderate densities. The inclusion of nucleon correlations is a difficult problem, extending far beyond the present work.

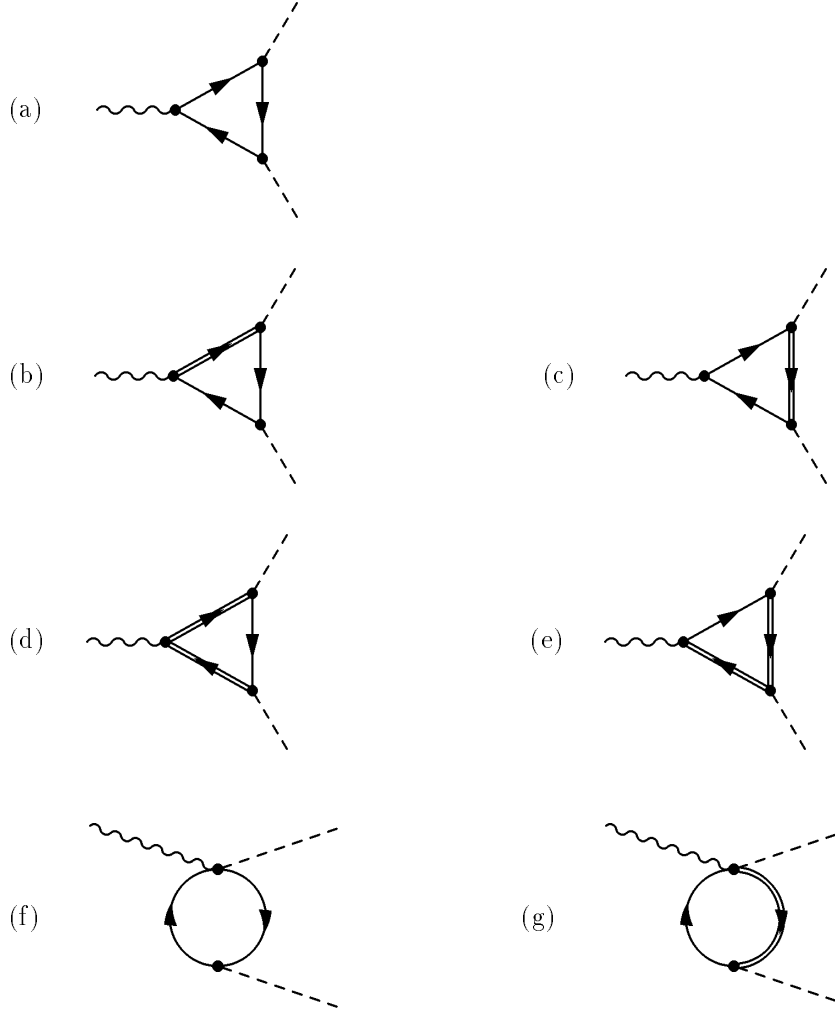


Fig. 1. Diagrams included in our calculation (crossed diagrams not displayed). Wavy lines denote the ρ meson, dashed lines the pions, solid lines the in-medium nucleon, and double lines the Δ .

$$-iV_{\pi^a NN} = \frac{g_A}{2F_\pi} \not{p} \gamma_5 \tau^a, \quad (4)$$

$$-iV_{\rho_\mu^b NN} = ig_\rho (\gamma^\mu + \frac{i\kappa_\rho}{2m_N} \sigma^{\mu\nu} q_\nu) \frac{\tau^b}{2}, \quad (5)$$

$$-iV_{\rho_\mu^b \pi^a NN} = i \frac{g_\rho g_A}{2F_\pi} \gamma^\mu \gamma_5 \varepsilon^{abc} \tau_c \quad (6)$$

where p is the outgoing four-momentum of the pion, q is the incoming momentum of the ρ meson, and a and b are the isospin indices of the pion and the ρ , respectively. We have chosen the pseudovector pion-nucleon coupling. The vertex (6) follows from the minimal substitution in Eq. (4).

Whereas the couplings of mesons to nucleons listed above are well established and the corresponding parameters are well known (except for the long-lasting controversy with κ_ρ), the relativistic couplings involving the Δ resonance are a topic of an on-going research and discussion [57,58,59,60]. Several structures are possible for these vertices, and ambiguities related to the choice of the so-called off-shell parameters have not been resolved. For our pragmatic goal of estimating the size of the in-medium $\rho\pi\pi$ vertex, we will adopt the following simple-minded and popular philosophy: all off-shell couplings are set to zero.

The meson-nucleon- Δ vertices have the following form [57]

$$-iV_{\pi^a N \Delta_\alpha} = \frac{f_{\pi N \Delta}}{m_\pi} \theta^{\alpha\nu}(Z) p_\nu T^a, \quad (7)$$

$$\begin{aligned} -iV_{\rho_\mu^b N \Delta_\alpha} &= ig_1 (\theta^{\mu\alpha}(Y) \not{q} \gamma_5 - \theta^{\mu\nu}(Y) q_\nu \gamma^\alpha \gamma_5) T^b \\ &\quad + ig_2 (\theta^{\mu\alpha}(X) \gamma_5 k \cdot q - \theta^{\mu\nu}(X) q_\nu \gamma_5 k^\alpha) T^b, \end{aligned} \quad (8)$$

$$-iV_{\rho_\mu^b \pi^a N \Delta_\alpha} = i \frac{g_\rho f_{\pi N \Delta}}{m_\pi} \theta^{\alpha\mu}(Z) \varepsilon^{abc} T_c, \quad (9)$$

where k is the nucleon four momentum, and

$$\theta^{\sigma\lambda}(W) = g^{\sigma\lambda} - (W + \frac{1}{2}) \gamma^\sigma \gamma^\lambda, \quad W = Z, Y, X. \quad (10)$$

The combination $-(W + \frac{1}{2})$ is called the off-shell parameter. According to the prescription stated above, we set $Z = Y = X = -\frac{1}{2}$, such that all off-shell parameters vanish, and we simply have $\theta^{\sigma\lambda}(W) = g^{\sigma\lambda}$. Furthermore, we take arbitrarily $g_2 = 0$. The matrices T^a in Eqs. (7-9) are the standard isospin $\frac{1}{2} \rightarrow \frac{3}{2}$ transition matrices, given in App. A. The vertex (9) follows from the minimum substitution in Eq. (7).

For the $\pi\Delta\Delta$ coupling there are, according to Ref. [59], three possible structures:

$$iV_{\pi^a \Delta_\alpha \Delta_\beta} = \left(G_1 g^{\alpha\beta} \not{p} \gamma_5 + G_2 (\gamma^\alpha p^\beta + p^\alpha \gamma^\beta) \gamma_5 + G_3 \gamma^\alpha \not{p} \gamma_5 \gamma^\beta \right) T_\Delta^a. \quad (11)$$

We drop the off-shell couplings by setting $G_2 = G_3 = 0$. For the $\rho\Delta\Delta$ vertex we use the minimal vector current coupling [57] and the universality prescription, which gives

$$iV_{\rho_\mu^b \Delta_\alpha \Delta_\beta} = ig_\rho (-\gamma^\mu g^{\alpha\beta} + g^{\alpha\mu} \gamma^\beta + g^{\beta\mu} \gamma^\alpha + \gamma^\alpha \gamma^\mu \gamma^\beta) T_\Delta^b. \quad (12)$$

The constants g_1 and G_1 are adjusted in such a way, that in the nonrelativistic limit we recover the couplings $\sqrt{2}(f^*/m_\pi)\varepsilon_{ijk}p^i S_\Delta^j T_\Delta^a$ and $(f_\Delta/m_\pi)p_j S_\Delta^j T_\Delta^a$, respectively [61,62], where k is the spin index of the ρ . The comparison, with the explicit form of the Rarita-Schwinger spinors and the matrices T_Δ and S_Δ (see

App. B) gives $G_1 = \frac{3}{2}f_\Delta/m_\pi$ and $g_1 = \sqrt{2}f^*/m_\pi$. Our choice of the physical parameters is as follows [62]:

$$\begin{aligned}
g_A &= 1.26, & F_\pi &= 93\text{MeV}, & m_\pi &= 139.6\text{MeV}, \\
g_\rho &= 5.26, & \kappa_\rho &= 6, \\
f_{\pi N\Delta} &= 2.12, & f^* &= 2.12, & f_\Delta &= 0.802.
\end{aligned}
\tag{13}$$

In addition to the mentioned ambiguities in the choice of the form of the Δ couplings [57,58,59,60], there are uncertainties in the values of the coupling constants. For some constants one typically uses the quark model predictions, or the large- N_c arguments which relate the Δ couplings to the nucleon couplings [63,64,65]. Any adopted scheme should fit the values of the coupling constants to the available data for various processes. However, for our purpose of estimating the size of the medium effect on the $\rho\pi\pi$ vertex these ambiguities are not essential. In addition, the result, as we shall see shortly, is dominated by diagram (g) of Fig. 1, containing only the $\pi N\Delta$ and $\pi\rho N\Delta$ couplings which are well established. Our results are not very sensitive to the choice of other couplings. Also, for simplicity of the approach and from the lack of knowledge we do not include any form-factors in the vertices.

We work in the rest frame of the nuclear matter, however effort is made to write all expressions covariantly, which turns out to be very convenient. Our calculation is made in the following way. First, we evaluate the diagrams of Fig. 1. The result for the full $\rho \rightarrow \pi\pi$ amplitude has the generic form $\mathcal{M}_{acb} = \varepsilon_\mu A_{acb}^\mu$, where the vertex function is

$$\begin{aligned}
A_{acb}^\mu &= \epsilon^{acb}(A_{\text{vac}}^\mu + A_{\text{med}}^\mu), \\
A_{\text{vac}}^\mu &= g_\rho(2p^\mu - q^\mu), \\
A_{\text{med}}^\mu &= \int \frac{d^3k}{(2\pi)^3} \frac{m_N}{E_k} (Ap^\mu + Bq^\mu + Ck^\mu)\theta(k_F - |\mathbf{k}|),
\end{aligned}
\tag{14}$$

and A , B , and C are scalar functions depending on scalar products of the four-vectors q , p , and k , with $k^0 = E_k$. The occupation function is made explicitly Lorentz-invariant when we write $|\mathbf{k}| = \sqrt{(k \cdot u)^2 - m_N^2}$, where u is the four-velocity of the medium. The term with k^μ , upon the evaluation of the integral, can be in general proportional to the three Lorentz vectors present in the problem, namely

$$\int \frac{d^3k}{(2\pi)^3} \frac{m_N}{E_k} Ck^\mu\theta(k_F - |\mathbf{k}|) = C_p p^\mu + C_q q^\mu + C_u u^\mu,
\tag{15}$$

where C_q , C_p , and C_u are scalar functions of p^2 , q^2 , $p \cdot q$, $p \cdot u$, $q \cdot u$, and k_F . Contracting Eq. (15) with p_μ , q_μ , and u_μ we obtain a set of linear algebraic

equations for C_q , C_p , and C_u , which can be solved. However, at the *leading-density* approximation the problem becomes even simpler. We can work in the *rest frame of the medium*, where $u^\mu = (1, 0, 0, 0)$. It is obvious that the leading-density approximation is equivalent to setting the three-vector \mathbf{k} to zero in the functions A , B , C , and E_k appearing in the integrands of Eqs. (14,15). Then $\int \frac{d^3k}{(2\pi)^3} \theta(k_f - |\mathbf{k}|) = \frac{1}{4}\rho_B$, while higher-order terms in \mathbf{k} generate terms with higher exponents of the baryon density ρ_B . Now, with $\mathbf{k} = 0$, $k^0 = m_N$, the contraction of Eq. (15) with q_μ , p_μ , and u_μ gives the set of equations

$$\begin{aligned}\frac{1}{4}\rho_B m_N p^0 \bar{C} &= C_p p^2 + C_q q \cdot p + C_u p^0, \\ \frac{1}{4}\rho_B m_N q^0 \bar{C} &= C_p p \cdot q + C_q q^2 + C_u q^0, \\ \frac{1}{4}\rho_B m_N \bar{C} &= C_p p \cdot u + C_q q \cdot u + C_u,\end{aligned}\tag{16}$$

where \bar{C} is C with $\mathbf{k} = 0$. Since in the general case vectors p , q , and u are linearly-independent, the solution of Eqs. (16) is $C_p = C_q = 0$, $C_u = \frac{1}{4}\rho_B m_N \bar{C}$. Thus, only the term proportional to u^μ in Eq. (15) is present in the leading-density approximation. In other words, we have

$$A_{\text{med}}^\mu = \frac{1}{4}\rho_B (\bar{A} p^\mu + \bar{B} q^\mu + \bar{C} m_N u^\mu),\tag{17}$$

where the coefficients \bar{A} , \bar{B} , and \bar{C} are obtained from A , B , and C by simply setting $\mathbf{k} = 0$.

To summarize this part, we restate the necessary steps needed to obtain the leading-density amplitude: The traces in diagrams of Fig. 1 are evaluated, leading to Eq. (14). Then we replace k^μ by $m_N u^\mu$, set $\mathbf{k} = 0$, and arrive at Eq. (17). Certainly, this very simple method is general for any problem involving baryon loops with density-dependent nucleon propagators. In our calculation we have used a standard Dirac algebra package [66]. The isospin traces are evaluated in App. B.

3 Results for ρ decaying at rest

We begin the presentation of the results with the case where the ρ is at rest with respect to nuclear matter, $\mathbf{q} = 0$. In this kinematics we find $\bar{B} = -\frac{1}{2}\bar{A}$, and $\bar{C} = 0$. The fact that $\bar{C} = 0$ is reflecting the equality of the transversely and longitudinally polarized ρ meson propagators at $\mathbf{q} = 0$, as will be shown in Sect. 4. The result $\bar{B} = -\frac{1}{2}\bar{A}$ is consistent with the Ward-Takahashi identity

$q_\mu A^\mu = D_\pi^{-1}(p) - D_\pi^{-1}(p - q)$, where D_π denotes the pion propagator dressed with nucleon and nucleon- Δ bubbles [7]. With $\mathbf{q} = 0$ and pions on the mass shell, we obviously have $D_\pi^{-1}(p) = D_\pi^{-1}(p - q)$, and, consequently, $\bar{A}p \cdot q + \bar{B}q^2 = 0$, which immediately gives $\bar{B} = -\frac{1}{2}\bar{A}$. Therefore, for $\mathbf{q} = 0$ the in-medium vertex function is proportional to $2p^\mu - q^\mu$:

$$A_{\text{med}}^\mu(\mathbf{q} = 0) = \frac{1}{8}\rho_B \bar{A}(\mathbf{q} = 0)(2p^\mu - q^\mu). \quad (18)$$

The full formula for $\bar{A}(\mathbf{q} = 0)$ is very lengthy, hence we present below only the contribution from the bubble diagrams (f,g), which are simple. In App. C we list the contributions to $\bar{A}(\mathbf{q} = 0)$ from all diagrams in the special case of $m_\pi = 0$.² It turns out that the $N - \Delta$ bubble diagram (g) is the dominant one. We have

$$\begin{aligned} \bar{A}^{(g)}(\mathbf{q} = 0) &= \frac{16}{9}g_\rho \left(\frac{f_{\pi N\Delta}}{m_\pi} \right)^2 \times \\ &\frac{2(m_\Delta^2 - m_\pi^2 - \frac{1}{2}m_N M)(m_N + m_\Delta + \frac{1}{2}M)}{m_\Delta^2(m_N^2 - (m_\Delta - \frac{i}{2}\Gamma_\Delta)^2 + m_\pi^2 + m_N M)} + (M \rightarrow -M), \end{aligned} \quad (19)$$

with M denoting the mass of the ρ meson. For comparison, the contribution from the $N - N$ bubble, Fig. 1(f), is

$$\bar{A}^{(f)}(\mathbf{q} = 0) = g_\rho \left(\frac{g_A}{2F_\pi} \right)^2 \frac{32m_N m_\pi^2}{m_\pi^4 - m_N^2 M^2}. \quad (20)$$

In the limit of large m_N , with $m_\Delta - m_N$ fixed, and $\Gamma_\Delta = 0$, expression (19) reduces to

$$\bar{A}^{(g)}(\mathbf{q} = 0) \rightarrow \frac{16}{9}g_\rho \left(\frac{f_{\pi N\Delta}}{m_\pi} \right)^2 \frac{4(m_\Delta - m_N)}{M^2/4 - (m_\Delta - m_N)^2}, \quad (21)$$

which agrees with non-relativistic calculations.

In the following we shall treat M as the mass of a *virtual* ρ meson. Virtual ρ mesons are needed for the analysis of the dilepton production in Sect. 5. Analyticity of the vertex function is nontrivial in the variable M . We can see from the denominators of Eqs. (19,20), that for $\Gamma_\Delta = 0$ singularities occur at

$$M^2 = \left(\frac{m_\Delta^2 - m_N^2 - m_\pi^2}{m_N} \right)^2 = (0.657\text{GeV})^2, \quad (22)$$

²It should be stressed that there is no obvious expansion parameter in the problem. Expanding the amplitude in m_π or $m_\Delta - m_N$ and keeping the lowest terms does not lead to a good approximation.

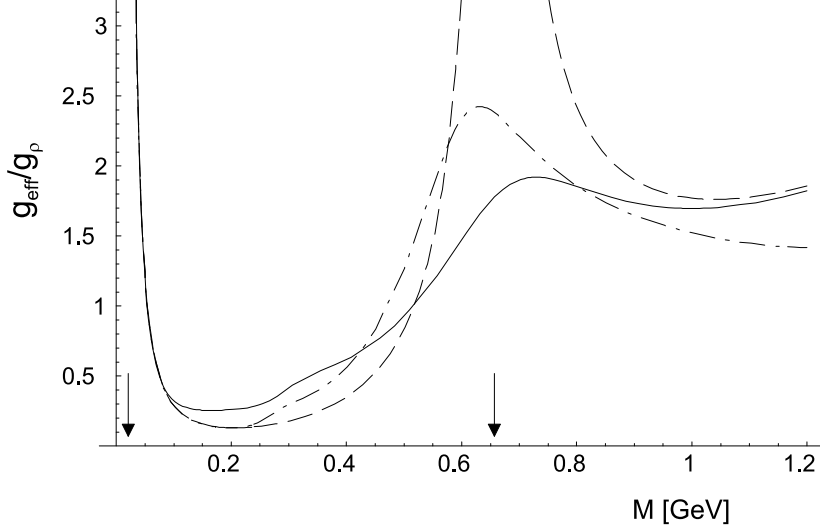


Fig. 2. The ratio of the effective coupling constant, Eq. (24), at the saturation density, to its vacuum value g_ρ , plotted as a function of the virtual mass of the ρ , M . The solid and dashed lines correspond to the case with $\Gamma_\Delta = 120\text{MeV}$ and $\Gamma_\Delta = 0$, respectively. The dot-dashed lines corresponds to the energy-dependent Γ_Δ of Eq. (25). Arrows indicate positions of the singularities of Eq. (22-23).

$$M^2 = \left(\frac{m_\pi^2}{m_N} \right)^2 = (0.021\text{GeV})^2. \quad (23)$$

Triangle diagrams of Fig. 1 also have the above singularities, and additionally bring in high-lying particle-antiparticle production singularities at $M^2 = (2m_N)^2$ and at $M^2 = (m_\Delta + m_N)^2$, which are physically not relevant. The above analytic structure is manifest in the numerical calculations presented below. For non-zero Γ_Δ the pole at (22) changes to a broader structure. Thus, analyticity is important — it immediately leads to large changes of the vertex function near the poles.

Since for the case of $\mathbf{q} = 0$ the matter-induced vertex function (18) has the same Lorentz structure as in the vacuum, *i.e.* proportional to $2p^\mu - q^\mu$, it is convenient for our quantitative studies to introduce an effective $\rho\pi\pi$ coupling constant, defined as

$$g_{\text{eff}} = \left| g_\rho + \frac{1}{8} \rho_B \bar{A}(\mathbf{q} = 0) \right|. \quad (24)$$

The absolute value is taken, since with non-zero Γ_Δ the quantity $\bar{A}(\mathbf{q} = 0)$ is complex. In Fig. 2 we plot the ratio g_{eff}/g_ρ as a function of the virtual ρ mass, M , at the saturation density, $\rho_B = \rho_0$. The dashed line corresponds to the zero-width Δ . We can clearly see the singularities of Eq. (22,23), whose positions are indicated by arrows. The solid line in Fig. 2 shows the calculation with the vacuum value of the Δ width, $\Gamma_\Delta = 120\text{MeV}$. In this case the pole at (22) changes

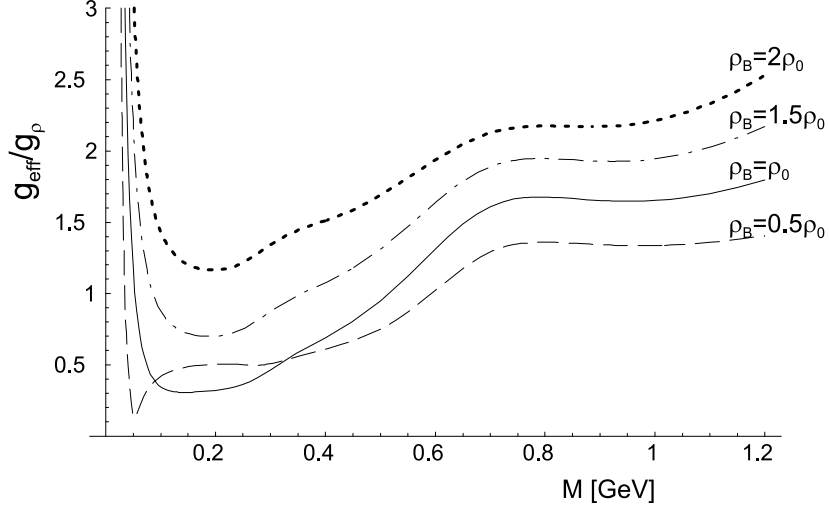


Fig. 3. Same as Fig. 2 for different values of the baryon density, ρ_B , with Γ_Δ depending on density according to parameterization (27).

to a broad structure. The pole of Eq. (23) remains, of course, unchanged. The considerable difference between the solid and dashed curves in the range of M between 0.6 and 1 GeV shows that the results are sensitive to the assumed value for Γ_Δ . We note that at low masses M , between ~ 0.07 and ~ 0.55 GeV, the effective coupling g_{eff} is lower than the vacuum value, thus the medium lowers the coupling, while above $M \sim 0.55$ GeV the effect is opposite: the coupling is increased. Around the physical ρ mass, $M = m_\rho$, the effective coupling is roughly two times larger than in the vacuum. For the width of the $\rho \rightarrow \pi\pi$ decay this means a factor of 4 enhancement, giving an in-medium width to the ρ of about 600 MeV at the saturation density. A similar estimate has been obtained *e.g.* in Refs. [23,29].

The dot-dashed line in Fig. 2 shows the result of a calculation with the energy-dependent width, parameterized as a function of the s variable as follows:

$$\Gamma_\Delta(s) = \Gamma_\Delta \left(\frac{q_{\text{cm}}(s)}{q_{\text{cm}}(m_\Delta)} \right)^3 \theta(s - (m_N + m_\pi)^2), \quad (25)$$

$$q_{\text{cm}}(s) = \frac{1}{2\sqrt{s}} \sqrt{(s - (m_N + m_\pi)^2)(s - (m_N - m_\pi)^2)}. \quad (26)$$

As can be seen from Fig. 2, the effects of energy-dependent widths are not large in our analysis.

It is interesting to look at the anatomy of the relative medium contribution to g_{eff} , *i.e.* of the quantity $\frac{1}{8}\rho_B \bar{A}(\mathbf{q} = 0)/g_\rho$. At $M = m_\rho = 776$ MeV and $\rho_B = \rho_0 = 0.17 \text{ fm}^{-3}$ we find that the diagrams (a)-(g) contribute, correspondingly, -0.08 , $0.22 - 0.09i$, $-0.008 - 0.008i$, $0.10 - 0.11i$, $-0.11 + 0.63i$, -0.008 , and $0.62 - 1.16i$,

with the total of $0.73 - 0.75i$, for the case $\Gamma_\Delta = 120\text{MeV}$, and $-.08, 0.33, 0.001, 0.25, -0.87, -0.008$, and 2.09 , with the total of 1.71 , for the case $\Gamma_\Delta = 0$. As advocated above, the largest contribution comes from the $N - \Delta$ bubble diagram (g).

In Fig. 3 we display the results for different values of the baryon density, ρ_B . In this study we have neglected the energy-dependence of the Δ width, but included the density dependence of Γ_Δ . The Δ broadens moderately at the nuclear saturation density [61,67], with Pauli blocking giving a decrease of Γ_Δ by about 40MeV , and absorption processes giving an increase by about 80MeV , such that the net effect is an increase by about 40MeV . Therefore we parameterize

$$\Gamma_\Delta(\rho_B) = \Gamma_\Delta \left(1 + \frac{40\text{MeV}}{\Gamma_\Delta} \frac{\rho_B}{\rho_0} \right). \quad (27)$$

Obviously, the effective coupling increases with ρ_B , as can be seen in Fig. 3. A caveat is in place here. Our method can be trusted numerically only at low values of the baryon density, such that the leading-density approximation holds. On the other hand we can see from Fig. 3 that the effects are large already at the saturation density, and certainly the approximation breaks down at larger values of ρ_B . Therefore our numerical results at high densities, here and in the following parts of the paper, have to be taken with a grain of salt and treated as indication of possible large effects rather than accurate numerical predictions.

Finally, we complete our discussion of the in-medium $\rho\pi\pi$ vertex at $\mathbf{q} = 0$ with Fig. 4, which shows the result of the calculation with fixed Γ_Δ , but with m_N and m_Δ scaled down to 70% of their vacuum values. A decrease of that order at the saturation density is anticipated from several approaches [1,3,68]. We notice that g_{eff} is enhanced and shifted to lower values of M when the baryon masses are rescaled.

4 Results for moving ρ

When the ρ meson moves with a non-zero momentum \mathbf{q} with respect to the medium, its propagation is different for transverse and longitudinal polarizations, defined by quantizing the spin along the direction of \mathbf{q} . To analyze this effect we shall consider the width of the transversely and longitudinally polarized ρ mesons due to the decay into two pions. This allows us to present the result in a more compact form, rather than looking separately at the functions \bar{A} , \bar{B} , and \bar{C} . The expression for the width for the decay $\rho^0 \rightarrow \pi^+\pi^-$, as viewed from the rest frame

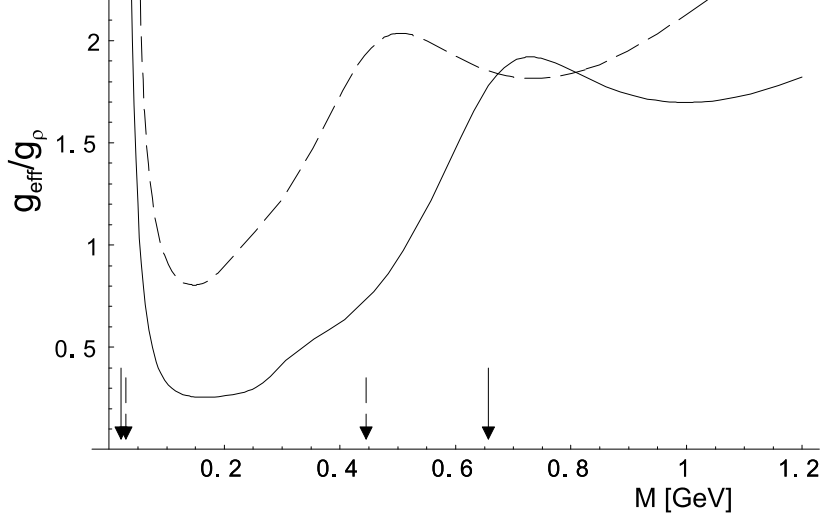


Fig. 4. Same as Fig. 2 for the vacuum values of the m_N and m_Δ (solid line), and for the values reduced to 70% (dashed line). Both curves evaluated at the baryon saturation density, and for $\Gamma_\Delta = 120\text{MeV}$.

of the medium, is

$$\Gamma_{\rho \rightarrow \pi\pi} = \frac{1}{n_s} \sum_s \frac{1}{2q_0} \int \frac{d^3p}{(2\pi)^3 2p_0} \int \frac{d^3p'}{(2\pi)^3 2p'_0} |\mathcal{M}|^2 (2\pi)^4 \delta^{(4)}(q - p - p'), \quad (28)$$

where n_s is the number of spin states of the ρ meson, and \sum_s denotes the sum over these spin states. The division by $q_0 = \sqrt{M^2 + \mathbf{q}^2}$ in Eq. (28), rather than by M , accounts for the time-dilatation effect. We perform the phase-space integral in the rest frame of the nuclear medium, and obtain

$$\Gamma_{\rho \rightarrow \pi\pi} = \frac{1}{n_s} \sum_s \frac{1}{2q_0} \sum_{b=1,2} \int_0^{\gamma^*} \sin \gamma \frac{(\mathbf{p}^{(b)})^2}{8\pi p_0^{(b)} (q_0 - p_0^{(b)}) |a^{(b)}|} |\mathcal{M}|^2 d\gamma, \quad (29)$$

where \sum_b is the sum over the two possible kinematic branches, which can appear when the two-body decay is viewed from a frame where the decaying particle moves. The angle γ is between the directions of \mathbf{q} and \mathbf{p} . The second branch appears only for $|\mathbf{q}|$ above a critical value,

$$|\mathbf{q}| > \frac{M\sqrt{M^2 - 4m_\pi^2}}{2m_\pi} \equiv q_{\text{crit}}. \quad (30)$$

Elementary kinematic considerations give

$$|\mathbf{p}^{(1,2)}| = \frac{M^2 |\mathbf{q}| \cos \gamma \pm q_0 \sqrt{M^4 - 4m_\pi^2 (M^2 + \mathbf{q}^2 \sin^2 \gamma)}}{2(M^2 + \mathbf{q}^2 \sin^2 \gamma)},$$

$$\begin{aligned}
q_0 &= \sqrt{M^2 + \mathbf{q}^2}, & p_0^{(1,2)} &= \sqrt{m_\pi^2 + (\mathbf{p}^{(1,2)})^2}, \\
a^{(1,2)} &= \frac{d(q_0 - \sqrt{m_\pi^2 + r^2} - \sqrt{m_\pi^2 + r^2 - 2r|\mathbf{q}|\cos\gamma + \mathbf{q}^2})}{dr} \Big|_{r=|\mathbf{p}^{(1,2)}|}, \\
\gamma^* &= \begin{cases} \pi & \text{for } q \leq q_{\text{crit}} \\ \arcsin\left(\frac{M\sqrt{M^2 - 4m_\pi^2}}{2m_\pi|\mathbf{q}|}\right) & \text{for } q > q_{\text{crit}} \end{cases}. \tag{31}
\end{aligned}$$

The transversely polarized ρ has two helicity states ($n_s = 2$), with projection $s = \pm 1$ on the direction of \mathbf{q} , described by polarization vectors $\varepsilon_{(\pm)}^\mu$, while the longitudinally polarized ρ has one helicity state ($n_s = 1$), with the corresponding projection $s = 0$, described by the polarization vector $\varepsilon_{(0)}^\mu$. An explicit calculation yields [49,69]

$$\begin{aligned}
-\varepsilon_{(+)}^{\mu*}\varepsilon_{(+)}^\nu - \varepsilon_{(-)}^{\mu*}\varepsilon_{(-)}^\nu &= g^{\mu\nu} - u^\mu u^\nu - \frac{(q^\mu - q \cdot u u^\mu)(q^\nu - q \cdot u u^\nu)}{q \cdot q - (q \cdot u)^2} \equiv T^{\mu\nu}, \\
-\varepsilon_{(0)}^{\mu*}\varepsilon_{(0)}^\nu &= -\frac{q^\mu q^\nu}{q \cdot q} + u^\mu u^\nu + \frac{(q^\mu - q \cdot u u^\mu)(q^\nu - q \cdot u u^\nu)}{q \cdot q - (q \cdot u)^2} \equiv L^{\mu\nu}. \tag{32}
\end{aligned}$$

Note that by summing over all polarizations one recovers the usual formula, *i.e.*

$$T^{\mu\nu} + L^{\mu\nu} = g^{\mu\nu} - \frac{q^\mu q^\nu}{q \cdot q}. \tag{33}$$

The tensors $T^{\mu\nu}$ and $L^{\mu\nu}$ are defined with such signs as to form projection operators, *i.e.*, $T^{\mu\nu}T_\nu^\alpha = T^{\mu\alpha}$, $L^{\mu\nu}L_\nu^\alpha = L^{\mu\alpha}$, and $T^{\mu\nu}L_\nu^\alpha = 0$. Furthermore, we have $T^{\mu\nu}q_\nu = 0$ and $L^{\mu\nu}q_\nu = 0$, which reflects current conservation, as well as $T^{\mu\nu}u_\nu = 0$. Through the use of these relation and Eqs. (14,17) we find that

$$|\mathcal{M}_T|^2 = \sum_{s=\pm} \varepsilon_{(s)}^{\mu*} A_\mu^* \varepsilon_{(s)}^\nu A_\nu = - \left| 2(g_\rho + \frac{1}{8}\rho_B \bar{A}) \right|^2 p_\mu T^{\mu\nu} p_\nu, \tag{34}$$

$$\begin{aligned}
|\mathcal{M}_L|^2 &= \sum_{s=0} \varepsilon_{(s)}^{\mu*} A_\mu^* \varepsilon_{(s)}^\nu A_\nu = \tag{35} \\
&- (2(g_\rho + \frac{1}{8}\rho_B \bar{A})^* p_\mu + \bar{C}^* m_N u_\mu) L^{\mu\nu} (2(g_\rho + \frac{1}{8}\rho_B \bar{A}) p_\nu + \bar{C} m_N u_\nu).
\end{aligned}$$

Note that the value of the coefficient \bar{B} in Eq. (17) is irrelevant for the widths. Equations (34,35) are used in Eq. (29).

Our numerical results are shown in Fig. 5. For simplicity, we have used here the constant $\Gamma_\Delta = 120\text{MeV}$. We notice considerable dependence on \mathbf{q} , as well as different behavior for the transverse and longitudinal cases. The transverse width

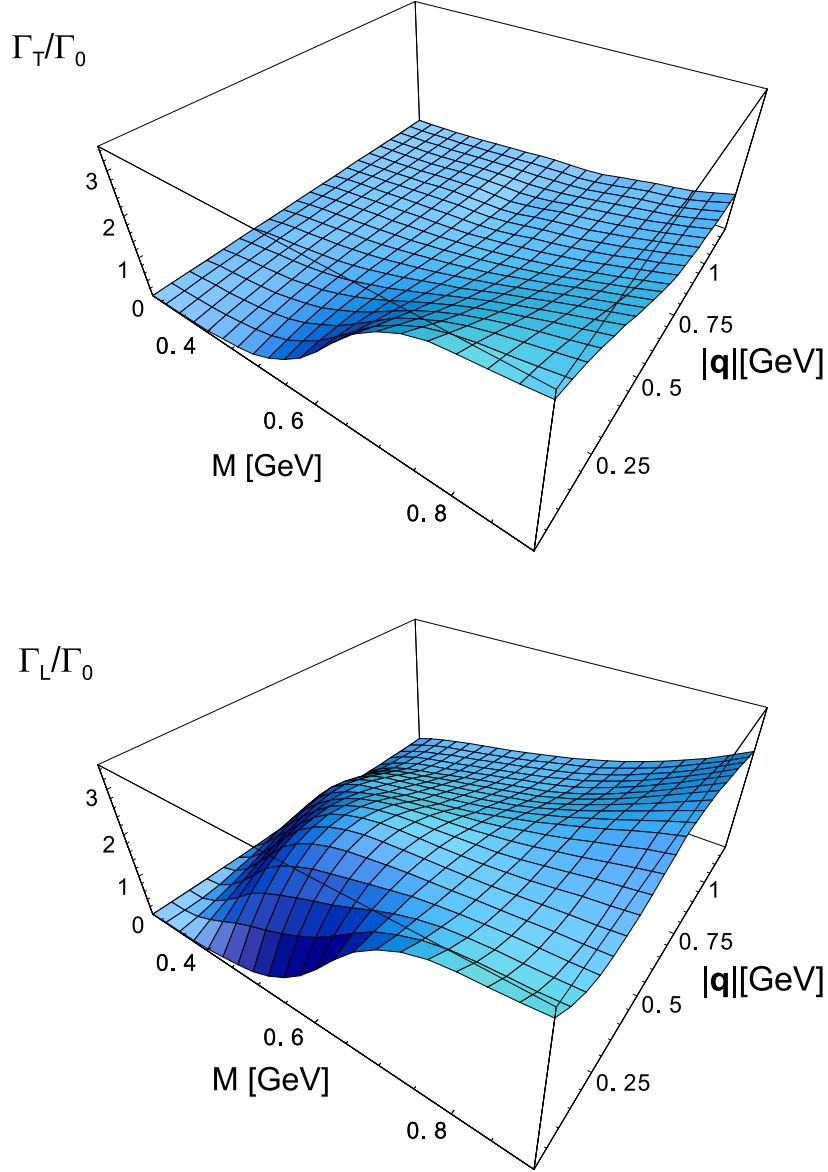


Fig. 5. The ratio of the width for the $\rho \rightarrow \pi\pi$ decay at the nuclear saturation density to its vacuum value, Γ_0 , plotted as a function of the virtual mass of the ρ , M , and the magnitude of its three-momentum with respect to nuclear matter, $|\mathbf{q}|$. Top: transverse polarization, bottom: longitudinal polarization.

decreases with $|\mathbf{q}|$, while the longitudinal does not. At lower values of M and $|\mathbf{q}|$ around 0.5GeV the longitudinal width develops a hill, absent in the transverse case.

The quantity which enters the formula for the dilepton production (see Sect. 5) is the spectral function of the transverse and longitudinal ρ mesons, defined as³

$$\mathcal{A}_P = \frac{1}{\pi} \frac{\sqrt{M^2 + \mathbf{q}^2} \Gamma_P}{(M^2 - m_\rho^2)^2 + (M^2 + \mathbf{q}^2) \Gamma_P^2}, \quad P = T, L, \quad (36)$$

where m_ρ is the position of the pole. The results for \mathcal{A}_T and \mathcal{A}_L , with $m_\rho = 776\text{MeV}$, are plotted in Fig. 6. We note that while at $\mathbf{q} = 0$ we obviously have $\mathcal{A}_T = \mathcal{A}_L$, at larger values of \mathbf{q} and at M around m_ρ the transverse spectral strength becomes dominant. At first glance this may seem surprising, since in Fig. 5 we have seen that at higher \mathbf{q} we have much larger Γ_L than Γ_T . However, the optimum value of Γ_P , at which \mathcal{A}_P has a maximum, is $\Gamma_P = (M^2 - m_\rho^2)/\sqrt{M^2 + \mathbf{q}^2}$. Lower, as well as higher values of Γ_P lead to a decrease in \mathcal{A}_P . This explains the behavior of Fig. 6. We note that the transverse spectral strength, \mathcal{A}_T , is concentrated along a ridge extending far into the large- \mathbf{q} region. Thus, a proper description of propagation at finite and large values of \mathbf{q} is needed for the description of ρ mesons in medium. We note that our results are in qualitative agreement with Ref. [11] (Fig. 14), with the somewhat different behavior of \mathcal{A}_T , which reaches larger values at higher values of $|\mathbf{q}|$ in our approach.⁴ We also find qualitative similarity to the results of the altogether different model of Ref. [15] (Figs. 6,7). There is a difference at larger values of $|\mathbf{q}|$ for \mathcal{A}_T , manifest in the presence of the rim in our Fig. 6. The results for \mathcal{A}_L are very similar to [15].

We should stress here that our construction of the ρ spectral function accounts only for the process $\rho \rightarrow \pi\pi$ and ignores all other possible contributions, such as *e.g.* from the s -channel resonances, studied in Refs. [14,15], medium modifications of the pions, *etc.* Such processes should be included in a more complete calculation. Still, the results of Sect. 5 depend only on the shape of the spectral functions of Fig. 6, and not on the physics leading to their form. Since the spectral functions obtained in many other approaches are quite similar to ours, the results obtained below can be viewed as representative to approaches containing the broadening of the ρ .

³ The presence of $\sqrt{M^2 + \mathbf{q}^2}$ here is related to the presence of $1/q_0$ in Eq.(29), *i.e.* to the fact that we are using widths viewed from the rest frame of the medium. Had we used widths viewed from the ρ rest frame, we would have $1/M$ in Eq.(29), and factors of M instead of $\sqrt{M^2 + \mathbf{q}^2}$ in Eq. (36). Of course, in both cases the resulting spectral functions are equal.

⁴ Note a factor of $1/\pi$ difference in our definition of the spectral functions compared to those of Ref. [11].

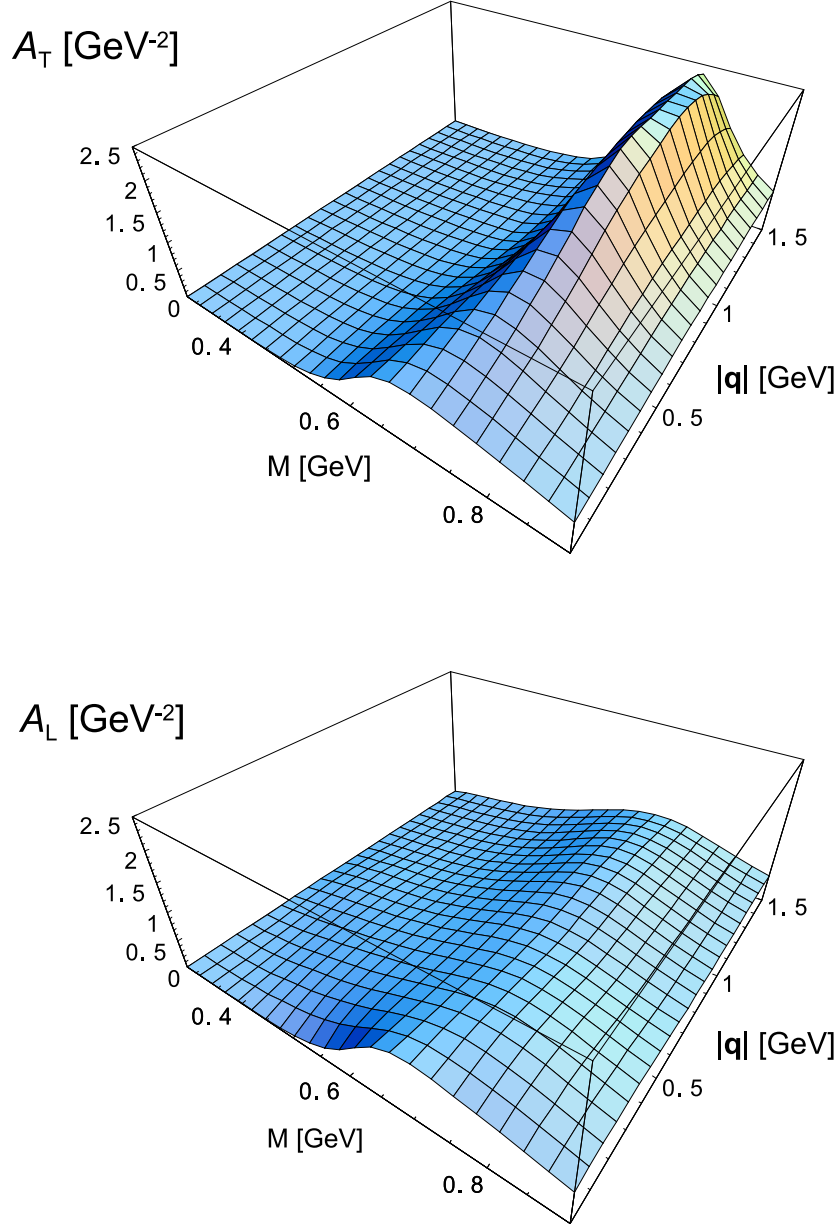


Fig. 6. The spectral strengths in the ρ channel at the nuclear saturation density, corresponding to the widths of Fig. 5. Top: transverse polarization, bottom: longitudinal polarization.

5 Dilepton production rate

Measurements of the low-mass dilepton spectra [40,41] have shown significant excess above yields from the final-state hadron decays. In this context, the properties of vector mesons (especially of the ρ) in a hadronic environment become of particular interest, since the Vector Meson Dominance Model is commonly used

to make the estimates of the dilepton yields from vector-meson decays. There are numerous analysis of the effect in the literature, both in hydrodynamic approaches [42,70,71,72,73], and in transport theories [13,74,75,76,77,78,79,80]. The dilepton-rate formula [81,82,83,84,85] from ρ meson decays can be written in a manifestly Lorentz covariant way as follows:

$$\frac{dN}{d^4x dM^2} = \int \frac{d^3q}{(2\pi)^3} \frac{M}{E_q} \Gamma_{\rho \rightarrow e^+e^-} \mathcal{A}(M, q \cdot u, \rho_B(x)) f_\rho \left(\frac{q \cdot u}{T(x)} \right), \quad (37)$$

where M is the invariant mass of the lepton pair, equal to the mass of the virtual ρ meson, $\mathcal{A} = 2\mathcal{A}_T + \mathcal{A}_L$ is the spectral function including all polarizations, x is a space-time point, $T(x)$ is the local value of temperature, and $E_q = \sqrt{M^2 + \mathbf{q}^2}$. The quantity $\Gamma_{\rho \rightarrow e^+e^-}$ in Eq. (37) is the width for the process $\rho \rightarrow e^+e^-$,

$$\Gamma_{\rho \rightarrow e^+e^-} = \frac{4\pi\alpha_{QED}^2 m_\rho^4}{3g_\rho^2 M^5} \left(1 - \frac{4m_e^2}{M^2} \right)^{\frac{1}{2}} (M^2 + 2m_e^2), \quad (38)$$

where α_{QED} is the fine structure constant, and m_e is the mass of the electron. Finally, the function f_ρ in Eq. (37) is the thermal Bose-Einstein distribution of the ρ mesons,

$$f_\rho = \left[\exp \left(\frac{q \cdot u - 2\mu_\pi}{T} \right) - 1 \right]^{-1}, \quad (39)$$

with μ_π denoting the pion chemical potential [85,86], incorporated in several works. This quantity in some sense mimics possible deviations of the system from the chemical equilibrium.

In order to describe the problem as realistically as possible, we will include the effects of the *expansion* of the medium formed in a relativistic heavy-ion collision. The lepton pairs are formed in a fire cylinder which moves as a whole in the lab system with the rapidity α_{FC} . For symmetric and central collisions α_{FC} is a half of the projectile rapidity in the lab. In its own center-of-mass system (CM), the fire cylinder undergoes a *hydrodynamic expansion*. In the analysis of such a situation, it is convenient to rewrite Eq. (37) in the variables suited to both the kinematics of the emission process and the geometry of the experimental setup. We introduce $M_\perp = \sqrt{M^2 + q_\perp^2}$, the transverse mass of the dilepton pair, y^{lab} , the rapidity of the pair measured in the lab system, \mathbf{u}_\perp , the transverse four-velocity of the fluid element producing dileptons, and α^{lab} , the rapidity of this fluid element in the lab. With these variables we have

$$q \cdot u = M_\perp \sqrt{1 + u_\perp^2} \cosh (y^{lab} - \alpha^{lab}) - \mathbf{q}_\perp \cdot \mathbf{u}_\perp. \quad (40)$$

The velocity of the fluid element in the lab is a relativistic superposition of the velocity of the fire cylinder in the lab and the hydrodynamic flow considered in

the CM system. Thus we have

$$\alpha^{lab} = \alpha + \alpha_{FC} = \operatorname{arctanh} v_{\parallel} + \alpha_{FC}, \quad u_{\perp} = \frac{v_{\perp} \cosh(\alpha)}{\sqrt{1 - v_{\perp}^2 \cosh^2(\alpha)}}. \quad (41)$$

We note that the velocities v_{\parallel} and v_{\perp} are defined now in the CM system. They depend on time and space coordinates.

Next, we analyze the kinematic constraint of the CERES experiment. The experimental acceptance cuts can be included with help of the function

$$\Phi(M, y^{lab}, q_{\perp}) = \frac{\int d^2 p_{1\perp} d^2 p_{2\perp} dy_1 dy_2 \phi \delta(E_q - E_{p_1} - E_{p_2}) \delta^{(3)}(\mathbf{q} - \mathbf{p}_1 - \mathbf{p}_2)}{\int d^2 p_{1\perp} d^2 p_{2\perp} dy_1 dy_2 \delta(E_q - E_{p_1} - E_{p_2}) \delta^{(3)}(\mathbf{q} - \mathbf{p}_1 - \mathbf{p}_2)}, \quad (42)$$

where $\mathbf{p}_{1,2}$ are the momenta of the emitted electrons, $y_{1,2}$ are the electron rapidities, and ϕ is a product of step functions which enforces the experimental setup conditions: $2.1 = \eta_{min} < y_{1,2} < \eta_{max} = 2.65$, $p_{1,2}^{\perp} > 200$ MeV, and $\theta_{ee} > 35$ mrad. Due to the smallness of the electron mass, we can assume here that rapidities and pseudorapidities of the electrons are equal. The construction of the function $\Phi(M, y^{lab}, q_{\perp})$ requires a numerical calculation of a two-dimensional integral of a function involving a product of step functions, which is very easily accomplished by a Monte Carlo method. With the inclusion of the experimental acceptance cuts, the dilepton production rate is

$$\frac{dN}{d^4x dM \Delta\eta} = \frac{2M^2}{(\eta_{max} - \eta_{min})} \int \frac{d^2 q_{\perp}}{(2\pi)^3} \int dy^{lab} \Phi \Gamma_{\rho \rightarrow e^+ e^-} \mathcal{A} f_{\rho}. \quad (43)$$

One should stress here the relevance of the inclusion of the kinematic cuts for the obtained results. The function Φ influences mostly the overall normalization of the cross section, and not so much the dependence on M .

In order to calculate the dilepton spectrum, one has to assume a model of the hydrodynamic expansion of the fire cylinder. We adopt the fire-cylinder expansion model of Refs. [54,55]. It is assumed that the system is in thermal equilibrium up to time t_{max} , when freeze-out occurs, and the velocities depend on space-time in the following way:

$$v_{\parallel}(t, z) = (v_z + a_z t) \frac{z}{z_{max}(t)}, \quad v_{\perp}(t, r) = (v_r + a_r t) \frac{r}{r_{max}(t)}, \quad (44)$$

where

$$z_{max}(t) = z_0 + v_z t + \frac{1}{2} a_z t^2, \quad r_{max}(t) = r_0 + v_r t + \frac{1}{2} a_r t^2 \quad (45)$$

are the boundaries of the system at time t . The parameters of the expansion are as follows [54,55]:

$$t_{max} = 11\text{fm}, \quad z_0 = 4.55\text{fm}, \quad r_0 = 4.6\text{fm}, \quad (46)$$

$$v_z = 0.5, \quad a_z = 0.023\text{fm}^{-1}, \quad v_r = 0, \quad a_r = 0.05\text{fm}^{-1}, \quad (47)$$

and the time dependences of the temperature and the baryon density are:

$$T(t) = 210\text{MeV} \exp\left(-\frac{t}{18.26\text{fm}}\right), \quad \rho_B(t) = 260/V(t), \quad (48)$$

where $V(t) = 2\pi z_{max}(t)r_{max}^2(t)$ is the volume of the fire cylinder at time t . For the time dependence of the pion chemical potential, $\mu_\pi(t)$, we assume a linear rise from 20MeV at $t = 0$ to 80MeV at $t = t_{max}$ [13].

Finally, the yield of leptons produced during the expansion is

$$\frac{dN_1}{dM\Delta\eta} = \int_0^{t_{max}} dt \int_0^{r_{max}(t)} 2\pi r dr \int_{-z_{max}(t)}^{z_{max}(t)} dz \left(\frac{dN}{d^4x dM\Delta\eta} \right), \quad (49)$$

where $dN/(d^4x dM\Delta\eta)$ is given by Eq. (43) with all the required substitutions.

In addition to the yields of Eq. (49) one usually adds the contribution from vector mesons which remain after freeze-out. This contribution is equal to

$$\frac{dN_2}{dM\Delta\eta} = \frac{1}{\Gamma(M)} \int_0^{r_{max}(t_{max})} 2\pi r dr \int_{-z_{max}(t_{max})}^{z_{max}(t_{max})} dz \left(\frac{dN}{d^4x dM\Delta\eta} \right), \quad (50)$$

where $\Gamma(M)$ is the *full* width of the ρ meson with virtual mass M , given by the formula

$$\Gamma(M) = \frac{g_{\rho\pi\pi}^2}{48\pi M^2} (M^2 - 4m_\pi^2)^{3/2} \quad (51)$$

with $g_{\rho\pi\pi} = 5.98$ giving $\Gamma(m_\rho) = 150\text{MeV}$. The physical interpretation of formula (50) is that all ρ mesons that remain after freeze-out, decay with the yield proportional to the number of mesons and the branching ratio to the dilepton channel. Finally, the full contribution is

$$\frac{dN}{dM\Delta\eta} = \frac{dN_1}{dM\Delta\eta} + \frac{dN_2}{dM\Delta\eta}. \quad (52)$$

Our numerical results are shown in Fig. 7. The solid line shows the yield from the ρ decays, Eq. (52), with the vacuum spectral strength of the ρ , while the

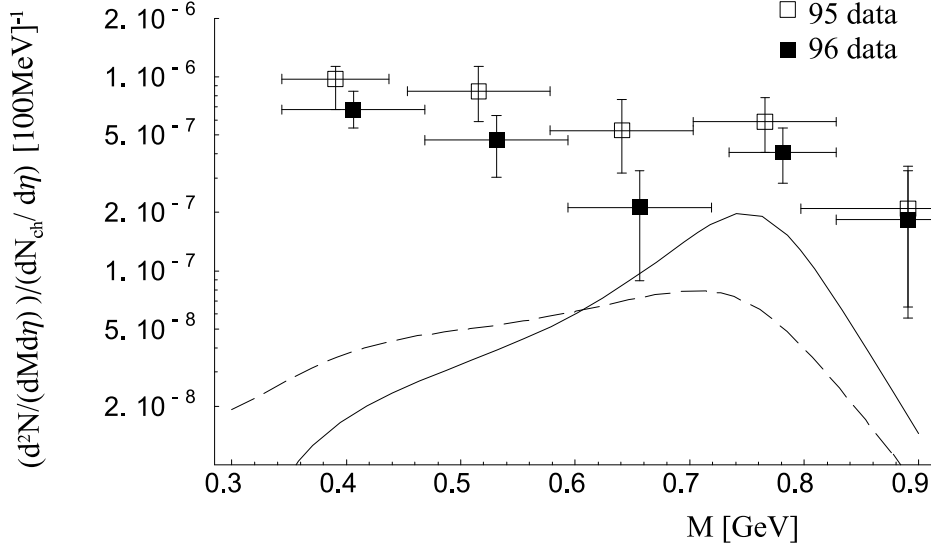


Fig. 7. Dilepton yields for the 158 GeV/A $Pb + Au$ CERES experiment from the ρ decays. The solid line is the result of the calculation with Eq. (49) and the vacuum ρ spectral function. The dashed line is obtained with the medium-modified spectral strength, Eq. (36). Contributions from other processes or the “cocktail” background are not included in the theoretical curves.

dashed curve shows the calculation with our medium-modified spectral strength of Eq. (36). We can see that the medium effects redistribute the dilepton yields from higher to lower values of M . This is a typical effect of broadening of the ρ , found in previous investigations. Thus the tendency needed to explain the experimental data is correct. We can see by comparing the dashed line to the data that the calculated yield falls an order of magnitude below the data. Note that other processes, not included in our calculation, contribute in the explored region of M , for instance the Dalitz decays of mesons, or the ω decays. Also, note that we are not including the “cocktail” contribution of decays of hadrons in our comparison, which would not be consistent. We have found that 15-25% of the model yields comes from decays after freeze-out. The effects of the expansion of the fire cylinder enhance the yields by a few percent. We stress that the overall normalization of the calculated curve is sensitive to the time-integrated volume of the fire cylinder, and to the hydrodynamic expansion parameters [87].

6 Summary and discussion

Here are the main conclusions of our investigation: the medium effects on the $\rho\pi\pi$ coupling are large, and dominantly come from the process where the Δ is excited in the intermediate state. At the nuclear saturation density and at physical mass of the ρ the value of the coupling is roughly doubled compared to the vacuum

value. The increased coupling leads directly to large widths of the ρ meson in medium. We have analyzed the resulting spectral functions for the transverse and longitudinal polarizations, with the result that at higher values of the three-momentum with respect to the medium, the transverse spectral function is much larger from the longitudinal one. Finally, we have applied our model to evaluate the dilepton production from the ρ decays in relativistic heavy-ion collisions. We confirm the well-known finding that a larger ρ width helps to understand the experimental data by redistributing strength from higher to lower invariant dilepton masses. However, the overall norm of the dilepton yields from the ρ decays is almost an order of magnitude too small to explain the experimental data. We remark that the results for the dilepton yields from ρ decays are only sensitive to the actual shape of the spectral functions and to the hydrodynamic expansion. In that sense they are not sensitive to detailed modelling of the dynamics, as long as the resulting functions \mathcal{A}_T and \mathcal{A}_L are similar. Thus our results confirm the statement of Ref. [87], namely that hydrodynamic models have problems in explaining the dilepton data unless the hydrodynamic evolution is exceedingly long.

For simplicity, we have used on-shell hadronic couplings throughout our studies. Since the nucleon and the Δ in the hadronic loop of Fig. 1 can be off-shell, additional coupling structures may be present. In addition, sideways form factors could be included for the particles off-shell. Presently, this has not been done, again for simplicity and from the lack of knowledge as to how to introduce and choose these form factors. One could also include the medium modifications of the meson-baryon couplings, a feature advocated, *e.g.*, in the model of Ref. [88,89].

The width of the ρ meson picks up contributions not only from the pion-loop diagram, included in our work, but also from other processes. In particular, one can include the s -channel resonances, as studied *e.g.* in Refs. [14,15]. Such processes can and should be included in a more complete and realistic calculation. Also the diagrams of Fig. 1 could in principle be supplied with higher resonances, at the expense of having more not well known parameters.

In addition to the effects of the Fermi sea, studied in this paper, *vacuum polarization* effects may influence the $\rho\pi\pi$ coupling. To have an estimate of these effects, we have done a Walecka-type calculation where in the diagrams of Fig. 1 we have included the *free* nucleon propagators only. We have found a $\sim 10\%$ increase of the coupling when the nucleon mass is reduced from 939MeV to 700MeV. We have applied Pauli-Villars regulator with the cut-off parameter of 1GeV in order to truncate high momenta in the loop. Similar order of the effect is found when the Nambu–Jona-Lasinio model is used along the lines of Ref. [90], and the mass of the quark is scaled down as expected from the medium effects. Thus, vacuum polarization effects on the $\rho\pi\pi$ coupling are estimated to be less significant than

the Fermi-sea effects presented in this paper.

Concerning the methods applied, we have shown in detail how to obtain very simply the leading-density approximation for diagrams involving loops with density-dependent nucleon propagators. We have also demonstrated how to carry a Lorentz-covariant calculation of the transverse and longitudinal spectral functions with help of the formulas of Sect. 4. These methods and formulas, although very straightforward, are not, to our knowledge, commonly know. They can be useful in studies similar to ours.

One of us (WF) thanks Dariusz Miśkowiec for a discussion of the CERES experimental cuts.

A Rarita-Schwinger spinors

The Rarita-Schwinger spinors are defined as

$$u^\mu(p, s_\Delta) = \sum_{\lambda, s_N} \langle 1 \frac{1}{2} \lambda s | 1 \frac{1}{2} \frac{3}{2} s_\Delta \rangle e^\mu(p, \lambda) u_\Delta(p, s), \quad (\text{A.1})$$

with

$$e^0(p, \lambda) = \frac{\vec{\varepsilon}_\lambda \cdot \vec{p}}{m_\Delta}, \quad e^i(p, \lambda) = \varepsilon_\lambda^i + \frac{(\vec{\varepsilon}_\lambda \cdot \vec{p}) p^i}{m_\Delta(E_\Delta + m_\Delta)}, \quad (\text{A.2})$$

$$E_\Delta = \sqrt{\vec{p}^2 + m_\Delta^2}. \quad (\text{A.3})$$

The polarization vectors are defined as

$$\vec{\varepsilon}_0 = \begin{pmatrix} 0 \\ 0 \\ 1 \end{pmatrix}, \quad \vec{\varepsilon}_\pm = \frac{1}{\sqrt{2}} \begin{pmatrix} \mp 1 \\ -i \\ 0 \end{pmatrix}, \quad (\text{A.4})$$

and

$$u_\Delta(p, s) = \sqrt{\frac{E_\Delta + m_\Delta}{2m_\Delta}} \begin{pmatrix} 1 \\ \frac{\vec{\sigma} \cdot \vec{p}}{E_\Delta + m_\Delta} \end{pmatrix} \chi(s), \quad (\text{A.5})$$

where $\chi(s)$ is the two-component spinor. The spinor $u^\mu(p, s_\Delta)$ satisfies the conditions $\gamma_\mu u^\mu(p, s_\Delta) = 0$ and $p_\mu u^\mu(p, s_\Delta) = 0$.

B Isospin algebra

The isospin $\frac{1}{2} \rightarrow \frac{3}{2}$ transition matrices are defined through the Clebsch-Gordan coefficients as follows: $\langle \frac{3}{2}, I_3 | T^\mu | \frac{1}{2}, i_3 \rangle = \langle \frac{1}{2} 1 i_3 \mu | 1 \frac{1}{2} \frac{3}{2} I_3 \rangle$, with i_3 and I_3 denoting the isospin of the nucleon and Δ , respectively. In Cartesian basis the explicit form reads

$$T^1 = \begin{pmatrix} -\frac{1}{\sqrt{2}} & 0 \\ 0 & -\frac{1}{\sqrt{6}} \\ \frac{1}{\sqrt{6}} & 0 \\ 0 & \frac{1}{\sqrt{2}} \end{pmatrix}, \quad T^2 = i \begin{pmatrix} \frac{1}{\sqrt{2}} & 0 \\ 0 & \frac{1}{\sqrt{6}} \\ \frac{1}{\sqrt{6}} & 0 \\ 0 & \frac{1}{\sqrt{2}} \end{pmatrix}, \quad T^3 = \begin{pmatrix} 0 & 0 \\ \sqrt{\frac{2}{3}} & 0 \\ 0 & \sqrt{\frac{2}{3}} \\ 0 & 0 \end{pmatrix}. \quad (\text{B.1})$$

where the columns are labeled by $i_3 = \frac{1}{2}, -\frac{1}{2}$, left to right, and the rows by $I_3 = \frac{3}{2}, \frac{1}{2}, -\frac{1}{2}, -\frac{3}{2}$, top to bottom. The following useful relation holds:

$$T^{a\dagger} T^b = \frac{2}{3} \delta^{ab} - \frac{1}{3} \varepsilon^{abc} \tau_c. \quad (\text{B.2})$$

The couplings of the Δ to the isovector proceed via the matrix T_Δ^μ defined as $\langle \frac{3}{2}, I_3' | T_\Delta^\mu | \frac{3}{2}, I_3 \rangle = \frac{\sqrt{15}}{2} \langle \frac{3}{2} 1 I_3' \mu | \frac{3}{2} \frac{1}{2} \frac{3}{2} I_3 \rangle$. Explicitly, we find

$$T_\Delta^1 = \begin{pmatrix} 0 & \frac{\sqrt{3}}{2} & 0 & 0 \\ \frac{\sqrt{3}}{2} & 0 & 1 & 0 \\ 0 & 1 & 0 & \frac{\sqrt{3}}{2} \\ 0 & 0 & \frac{\sqrt{3}}{2} & 0 \end{pmatrix}, \quad T_\Delta^2 = i \begin{pmatrix} 0 & -\frac{\sqrt{3}}{2} & 0 & 0 \\ \frac{\sqrt{3}}{2} & 0 & -1 & 0 \\ 0 & 1 & 0 & -\frac{\sqrt{3}}{2} \\ 0 & 0 & \frac{\sqrt{3}}{2} & 0 \end{pmatrix},$$

$$T_\Delta^3 = \begin{pmatrix} \frac{3}{2} & 0 & 0 & 0 \\ 0 & \frac{1}{2} & 0 & 0 \\ 0 & 0 & -\frac{1}{2} & 0 \\ 0 & 0 & 0 & -\frac{3}{2} \end{pmatrix}, \quad (\text{B.3})$$

where the columns are labeled by $I_3' = \frac{3}{2}, \frac{1}{2}, -\frac{1}{2}, -\frac{3}{2}$, left to right, and the rows by $I_3 = \frac{3}{2}, \frac{1}{2}, -\frac{1}{2}, -\frac{3}{2}$, top to bottom. The conventional factor of $\sqrt{15}/2$ in the definition ensures that T_Δ^3 simply measures the third component of the isospin of the Δ . The spin coupling matrices used in non-relativistic calculations, S^i and S_Δ^i , are defined analogously and have exactly the same values as T^a and T_Δ^a .

Isospin trace factors for diagrams of Fig. 1 can be now readily obtained. They are equal to 2, $-\frac{2}{3}$, $-\frac{2}{3}$, $\frac{5}{3}$, $\frac{5}{3}$, 2, and $\frac{4}{3}$ times $-i\epsilon^{acb}$, for diagrams (a),(b),..., (g),

respectively. Isospin indices a , b , and c have the assignment as specified on the text above Eq. (1).

C Amplitudes for $\mathbf{q} = 0$

For the case $\mathbf{q} = 0$ the amplitude corresponding to the diagram (i) of Fig. 1 can be written as

$$A_{(i)}^\mu = \frac{1}{8} \rho_B G_{(i)} \frac{N_{(i)}}{D_{(i)}} (2p^\mu - q^\mu), \quad (\text{C.1})$$

where $G_{(i)}$ are products of coupling constants:

$$\begin{aligned} G_{(a)} &= \frac{g_A^2 g_\rho}{8F_\pi^2}, & G_{(b)} &= \frac{\sqrt{2} g_A f^* f_{\pi N \Delta}}{2F_\pi m_\pi^2}, & G_{(c)} &= \frac{g_\rho f_{\pi N \Delta}^2}{2m_\pi^2}, \\ G_{(d)} &= \frac{g_\rho f_{\pi N \Delta}^2}{m_\pi^2}, & G_{(e)} &= \frac{3\sqrt{2} f^* f_{\pi N \Delta} f_\Delta}{2m_\pi^3}, & G_{(f)} &= \frac{g_\rho g_A^2}{4F_\pi^2}, \\ G_{(g)} &= \frac{g_\rho f_{\pi N \Delta}^2}{m_\pi^2}. \end{aligned} \quad (\text{C.2})$$

The formulas for $N_{(i)}$ and $D_{(i)}$ are very long in the general case, which reflects the presence of many terms in the Rarita-Schwinger propagator. Numerators $N_{(i)}$ become manageable in the formal case $\Gamma_\Delta = 0$, and $m_\pi = 0$, where we find

$$\begin{aligned} N_{(a)} &= -8 \left(4 m_N^4 M^2 + \kappa_\rho m_N^2 M^4 \right), \\ N_{(b)} &= 16 m_N^2 (m_N + m_\Delta - M) M^2 (m_N + m_\Delta + M) \\ &\quad \left(2 m_N^4 + m_N^3 m_\Delta - m_N m_\Delta^3 + 2 m_\Delta^4 - 2 m_N^2 (2 m_\Delta^2 + M^2) \right), \\ N_{(c)} &= -16 m_N (m_N - m_\Delta) (m_N + m_\Delta) \\ &\quad \left(m_N^3 - (1 + \kappa_\rho) m_N^2 m_\Delta - 2 m_N m_\Delta^2 + (1 + \kappa_\rho) m_\Delta^3 \right) M^2 - \\ &\quad 4 \left(\begin{array}{l} (-4 + \kappa_\rho) m_N^4 + 4 (1 + \kappa_\rho) m_N^3 m_\Delta - \\ (2 + 5 \kappa_\rho) m_N^2 m_\Delta^2 + 2 \kappa_\rho m_\Delta^4 \end{array} \right) M^4 + 4 \kappa_\rho m_N^2 M^6, \\ N_{(d)} &= -20 M^2 \left(4 m_N^3 m_\Delta - m_N m_\Delta^3 - 4 m_\Delta^4 + m_N^2 (7 m_\Delta^2 + M^2) \right), \end{aligned}$$

$$\begin{aligned}
N_{(e)} &= 40 M^2 \left(\begin{array}{l} (m_N - m_\Delta) (m_N + m_\Delta)^3 \left(\begin{array}{l} 2 m_N^4 + 4 m_N^3 m_\Delta - \\ 2 m_N m_\Delta^3 - 7 m_\Delta^4 \end{array} \right) - \\ (m_N + m_\Delta) \left(\begin{array}{l} 3 m_N^5 + 7 m_N^4 m_\Delta + 4 m_N^3 m_\Delta^2 + \\ m_N^2 m_\Delta^3 - 2 m_N m_\Delta^4 + 2 m_\Delta^5 \end{array} \right) M^2 + \\ m_\Delta (m_N + m_\Delta) (2 m_N^2 + m_N m_\Delta - 2 m_\Delta^2) M^4 + m_N^2 M^6 \end{array} \right), \\
N_{(f)} &= 0, \\
N_{(g)} &= 16 \left(\begin{array}{l} 4 (m_N - m_\Delta) m_\Delta^2 (m_N + m_\Delta)^2 + \\ m_N (m_N^2 + 2 m_N m_\Delta - m_\Delta^2) M^2 \end{array} \right). \tag{C.3}
\end{aligned}$$

The expressions for $D_{(i)}$ for the case $\Gamma_\Delta = 0$ are

$$\begin{aligned}
D_{(a)} &= (4 m_N^3 - m_N M^2) (-m_\pi^4 + m_N^2 M^2), \\
D_{(b)} &= 9 m_\Delta^2 (m_N + m_\Delta - M) (m_N + m_\Delta + M) (m_N^2 - m_\Delta^2 + m_\pi^2 - m_N M) \\
&\quad \times (-m_\pi^2 + m_N M) (m_\pi^2 + m_N M) (-m_\Delta^2 + m_\pi^2 + m_N (m_N + M)), \\
D_{(c)} &= 9 m_\Delta^2 (-4 m_N^3 + m_N M^2) \left((m_N^2 - m_\Delta^2 + m_\pi^2)^2 - m_N^2 M^2 \right), \\
D_{(d)} &= 27 m_\Delta^3 \left((m_N^2 - m_\Delta^2 + m_\pi^2)^2 - m_N^2 M^2 \right), \\
D_{(e)} &= 27 m_\Delta^4 (m_N + m_\Delta - M) (m_N + m_\Delta + M) \times \\
&\quad \left((m_N^2 - m_\Delta^2 + m_\pi^2)^2 - m_N^2 M^2 \right), \\
D_{(f)} &= m_\pi^4 - m_N^2 M^2, \\
D_{(g)} &= 9 m_\Delta^2 \left((m_N^2 - m_\Delta^2 + m_\pi^2)^2 - m_N^2 M^2 \right). \tag{C.4}
\end{aligned}$$

References

- [1] G. E. Brown and M. Rho, Phys. Rev. Lett. **66** (1991) 2720
- [2] L. S. Celenza, A. Pantziris, C. M. Shakin, and W.-D. Sun, Phys. Rev. **C45** (1992) 2015
- [3] B. D. Serot and J. D. Walecka, Advances in Nuclear Physics **16** (1986) 1
- [4] S. A. Chin, Ann. Phys. (NY) **108** (1977) 301
- [5] T. Hatsuda, H. Shiomi, and H. Kuwabara, Prog. Theor. Phys. **95** (1996) 1009
- [6] H.-C. Jean, J. Piekarewicz, and A. G. Williams, Phys. Rev. **C49** (1994) 1981
- [7] M. Herrmann, B. L. Friman, and W. Noerenberg, Nucl. Phys. **A560** (1993) 411
- [8] M. Herrmann, B. L. Friman, and W. Noerenberg, Nucl. Phys. **A545** (1992) 267C
- [9] M. Herrmann, B. L. Friman, and W. Noerenberg, Z. Phys. **A343** (1992) 119
- [10] B. Friman and H. J. Pirner, Nucl. Phys. **A617** (1997) 496
- [11] M. Urban, M. Buballa, R. Rapp, and J. Wambach, Nucl. Phys. **A641** (1998) 433
- [12] M. Urban, M. Buballa, R. Rapp, and J. Wambach, Nucl. Phys. **A673** (2000) 357
- [13] R. Rapp, G. Chanfray, and J. Wambach, Nucl. Phys. **A617** (1997) 472
- [14] M. Post, S. Leupold, and U. Mosel, preprint (2000), nucl-th/0008027
- [15] W. Peters, M. Post, H. Lenske, S. Leupold, and U. Mosel, Nucl. Phys. **A632** (1998) 109
- [16] S. Leupold and U. Mosel, Prog. Part. Nucl. Phys. **42** (1999) 221
- [17] S. Gao, C. Gale, C. Ernst, H. Stocker, and W. Greiner, Nucl. Phys. **A661** (1999) 518
- [18] T. Hatsuda and S. H. Lee, Phys. Rev. **C46** (1993) R34
- [19] S. Leupold, W. Peters, and U. Mosel, Nucl. Phys. **A628** (1998) 311
- [20] S. H. Lee, Nucl. Phys. **A670** (2000) 119
- [21] T. Hatsuda and T. Kunihiro, Phys. Rept. **247** (1994) 221
- [22] U. Vogl and W. Weise, Prog. Part. Nucl. Phys. **27** (1991) 195
- [23] F. Klingl, N. Kaiser, and W. Weise, Nucl. Phys. **A624** (1997) 527
- [24] D. Cabrera, E. Oset, and M. J. Vicente-Vacas, preprint (2000), nucl-th/0011037

- [25] D. Cabrera, E. Oset, and M. J. Vicente-Vacas, *Acta Phys. Polon.* **B31** (2000) 2167
- [26] G. Chanfray, *Nucl. Phys.* **A685** (2001) 328
- [27] W. Broniowski and B. Hiller, *Phys. Lett.* **B392** (1997) 267
- [28] W. Broniowski and B. Hiller, *Nucl. Phys.* **A643** (1998) 161
- [29] V. L. Eletsky, B. L. Ioffe, and J. I. Kapusta, *Eur. J. Phys.* **A3** (1998) 381
- [30] B. Friman, *Acta Phys. Polon.* **B29** (1998) 3195
- [31] M. Lutz, B. Friman, and G. Wolf, *Nucl. Phys.* **A661** (1999) 526
- [32] B. Friman, M. Lutz, and G. Wolf, preprint (2000), nucl-th/0003012
- [33] *Hadrons in Nuclear Matter*, edited by H. Feldmaier and W. Noerenberg (GSI, Darmstadt, 1995), proc. Int. Workshop XXIII on Gross Properties of Nuclei and Nuclear Excitations, Hirschegg, Austria, 1995
- [34] Quark matter '97. Ultra-relativistic nucleus nucleus collisions. Proceedings, 48th Yamada Conference, 13th International Conference, Tsukuba, Japan, December 1-5, 1997, edited by T. Hatsuda, Y. Miake, K. Yagi, and S. Nagamiya, *Nucl. Phys.* **A638** (1998) 1
- [35] Quark matter '99. Proceedings, 14th International Conference on ultra-relativistic nucleus nucleus collisions, Torino, Italy, May 10-15, 1999, edited by L. Riccati, M. Maserà, and E. Vercellin, *Nucl. Phys.* **A661** (1999) 1
- [36] A. K. Dutt-Mazumder, B. Dutta-Roy, and A. Kundu, *Phys. Lett.* **B399** (1997) 196
- [37] W. Broniowski and W. Florkowski, *Phys. Lett.* **B440** (1998) 7
- [38] A. K. Dutt-Mazumder, C. Gale, and O. Teodorescu, preprint (2000), nucl-th/0008056
- [39] O. Teodorescu, A. K. Dutt-Mazumder, and C. Gale, *Phys. Rev.* **C63** (2001) 034903
- [40] CERES Collab., G. Agakichiev *et al.*, *Phys. Rev. Lett.* **75** (1995) 1272
- [41] HELIOS/3 Collab., M. Maserà *et al.*, *Nucl. Phys.* **A590** (1995) 93c
- [42] C. A. Dominguez and M. Loewe, *Z. Phys.* **C49** (1991) 423
- [43] G. Q. Li, C. M. Ko, and G. E. Brown, *Phys. Rev. Lett.* **75** (1995) 4007
- [44] G. Q. Li, C. M. Ko, and G. E. Brown, *Nucl. Phys.* **A606** (1996) 568
- [45] E. L. Bratkovskaya and C. M. Ko, *Phys. Lett.* **B445** (1999) 265
- [46] G. Q. Li, G. E. Brown, C. Gale, and C. M. Ko, preprint (1997), nucl-th/9712048
- [47] R. Rapp and J. Wambach, *Adv. Nucl. Phys* **25** (2000) 1

- [48] C. Song and V. Koch, Phys. Rev. **C54** (1996) 3218
- [49] W. Broniowski, W. Florkowski, and B. Hiller, Acta Phys. Polon. **B30** (1999) 1079
- [50] W. Broniowski, W. Florkowski, and B. Hiller, Eur. Phys. J. **A7** (2000) 287
- [51] W. Broniowski, W. Florkowski, and B. Hiller, in *Hadron Physics: Effective theories of low-energy QCD, Coimbra, Portugal, September 1999, AIP Conference Proceedings*, edited by A. H. Blin *et al.* (AIP, Melville, New York, 2000), Vol. 508, p. 218, nucl-th/9910057
- [52] B. Krippa, Nucl. Phys. **A672** (2000) 270
- [53] M. C. Ruivo, C. A. de Sousa, B. Hiller, and A. H. Blin, Nucl. Phys. **A575** (1994) 460
- [54] R. Rapp and J. Wambach, Eur. Phys. J. **A6** (1999) 415
- [55] R. Rapp and E. Shuryak, Phys. Lett. **B473** (2000) 13
- [56] W. Rarita and J. Schwinger, Phys. Rev. **60** (1941) 61
- [57] M. Benmerrouche, R. M. Davidson, and N. C. Mukhopadhyay, Phys. Rev. **C39** (1989) 2339
- [58] V. Pascalutsa and R. Timmermans, Phys. Rev. **C60** (1999) 042201
- [59] T. R. Hemmert, B. R. Holstein, and J. Kambor, J. Phys. G **G24** (1998) 1831
- [60] H. Haberzettl, preprint (1998), nucl-th/9812043
- [61] T. O. E. Ericson and W. Weise, *Pions and nuclei* (Clarendon Press, Oxford, 1988)
- [62] J. A. G. Tejedor and E. Oset, Nucl. Phys. **A571** (1994) 667
- [63] R. Dashen and A. V. Manohar, Phys. Lett. **B315** (1993) 425
- [64] R. Dashen and A. V. Manohar, Phys. Lett. **B315** (1993) 438
- [65] W. Broniowski, Nucl. Phys. **A580** (1994) 429
- [66] A. Hsieh and E. Yehudai, Comput. Phys. **6** (1992) 253
- [67] F. Osterfeld and B. Koerfgen, Nucl. Phys. **A599** (1996) 129C
- [68] T. D. Cohen, R. J. Furnstahl, and D. K. Griegel, Phys. Rev. **C45** (1992) 1881
- [69] W. Florkowski and W. Broniowski, Nucl. Phys. **A651** (1999) 397
- [70] D. K. Srivastava, B. Sinha, and C. Gale, Phys. Rev. **C53** (1996) 567
- [71] C. M. Hung and E. V. Shuryak, Phys. Rev. **C56** (1997) 453
- [72] J. Sollfrank, P. Huovinen, M. Kataja, P. V. Ruuskanen, M. Prakash, and R. Venugopalan, Phys. Rev. **C55** (1997) 392

- [73] R. Baier, M. Dirks, and K. Redlich, Phys. Rev. **D55** (1997) 4344
- [74] V. Koch and C. Song, Phys. Rev. **C54** (1996) 1903
- [75] G. Q. Li, C. M. Ko, and G. E. Brown, Nucl. Phys. **A606** (1996) 568
- [76] G. Q. Li, C. M. Ko, and G. E. Brown, Phys. Rev. Lett. **75** (1995) 4007
- [77] W. Cassing, W. Ehehalt, and C. M. Ko, Phys. Lett. **B363** (1995) 35
- [78] R. Rapp, G. Chanfray, and J. Wambach, Phys. Rev. Lett. **76** (1996) 368
- [79] H. J. Schulze and D. Blaschke, Phys. Lett. **B386** (1996) 429
- [80] J. V. Steele, H. Yamagishi, and I. Zahed, Phys. Lett. **B384** (1996) 255
- [81] C. Gale and J. Kapusta, Phys. Rev. **C35** (1987) 2107
- [82] C. Gale and J. Kapusta, Nucl. Phys. **B357** (1991) 65
- [83] C. L. Korpa and S. Pratt, Phys. Rev. Lett. **64** (1990) 1502
- [84] H. A. Weldon, Z. Phys. **C54** (1992) 431
- [85] P. Koch, Z. Phys. **C57** (1993) 283
- [86] P. Koch, Phys. Lett. **B288** (1992) 187
- [87] C. M. Hung and E. V. Shuryak, Phys. Rev. Lett. **75** (1995) 4003
- [88] M. K. Banerjee, Phys. Rev. **C45** (1992) 1359
- [89] M. K. Banerjee and J. A. Tjon, Phys. Rev. **C56** (1997) 497
- [90] V. Bernard, A. H. Blin, B. Hiller, Yu. P. Ivanov, A. A. Osipov, and U.-G. Meißner, Ann. Phys. (NY) **249** (1996) 499